NMR IN BIOMEDICINE
NMR Biomed. 2003;**16**:67–76
Published online in Wiley InterScience (www.interscience.wiley.com). DOI:10.1002/nbm.813

Evaluation of (*E*)-2′-deoxy-2′-(fluoromethylene)cytidine on the 9L rat brain tumor model using MRI

Brian D. Ross,[1]* Thomas L. Chenevert,[1] Michael Garwood,[2] Boklye Kim,[1] Lauren D. Stegman,[1] Oded Ben-Yoseph,[1] John Zwolshen,[3] Alnawaz Rehemtulla[4] and Prasad S. Sunkara[5]

[1]Department of Radiology, Center for Molecular Imaging, University of Michigan, Ann Arbor, MI 48109, USA
[2]Department of Radiology, Center for Magnetic Resonance Research and Cancer Center, University of Minnesota, Minneapolis, MN 55456, USA
[3]Raymond Walters College, Cincinnati, OH 45236, USA
[4]Department of Radiation Oncology, University of Michigan, Ann Arbor, MI 48109, USA
[5]Molecular Therapeutics Inc., Ann Arbor, MI 48104, USA

Received 1 July 2002; Revised 15 October 2002; Accepted 20 November 2002

ABSTRACT: (*E*)-2′-deoxy-2′-(fluoromethylene)cytidine (FMdC), was evaluated as a potential treatment for malignant gliomas using the rat 9L brain tumor model. FMdC was shown to be an effective inhibitor of cell proliferation in cultured 9L cells with an EC_{50} of 40 ng/ml. *In vitro* studies also revealed that this compound significantly inhibited incorporation of [^{3}H]thymidine in 9L cells. *In vivo* therapeutic efficacy of FMdC was evaluated in rats harboring intracerebral 9L tumors which were treated daily with 15 mg/kg, i.p. Treatment response was quantified from changes in tumor growth rates as assessed from sequential magnetic resonance imaging (MRI) tumor volume measurements. *In vivo* tumor cell kill in individual animals was calculated by fitting tumor volume data with an iterative computer routine. It was estimated that therapeutically responsive rats treated with FMdC daily produced a ≥ 0.1 log kill per therapeutic dose which resulted in a significant reduction in tumor growth rate. In addition, localized ^{1}H-MRS of intracerebral 9L tumors revealed changes in metabolite levels which correlated with therapeutic response. These results provide evidence supporting the use of FMdC in clinical trials for the treatment of malignant gliomas and reveals that MR can play an important role in the pre-clinical evaluation of novel compounds using orthotopic tumor models. Copyright © 2003 John Wiley & Sons, Ltd.

KEYWORDS: 9L glioma; MRI; proton MRS; cell kill; fluoromethylene-2′-deoxycytidine

INTRODUCTION

There has been little progress in improving the long-term survival rate of patients with malignant gliomas over the last two decades. Surgical resection and radiation therapy are the most beneficial forms of treatment, achieving a median survival time of only 9 months with few long-term survivors.[1] Adjuvant chemotherapy with nitrosourea-based regimens prolongs median survival by 2 months and provides a minimal increase in patient survival at one year.[2] Treatment failure and patient mortality is almost exclusively due to local recurrence. This has prompted investigational treatments aimed at improving local control including gene therapy and intracavitary chemotherapy.[3] Although these local therapies may hold promise, it is clear that the discovery of novel, active chemotherapeutic agents is also required to improve clinical outcomes.

One such potential agent is (E)-2′-deoxy-2′-(fluoromethylene) cytidine (FMdC, tezacitabine, MDL-101731), a novel deoxycytidine analog with potent anticancer activity. FMdC was originally developed as a specific inhibitor of ribonucleotide reductase.[4] Although its anticancer activity is partly attributable to mechanism-based inhibition of ribonucleotide reductase,[5] recent work suggests that termination of DNA synthesis by incorporated FMdC is the predominant molecular event responsible for its cytotoxicity.[6] Pre-clinical studies of FMdC have demonstrated potent activity against human breast cancer xenografts,[7] human colon and prostate tumor xenografts,[8,9] as well as human neuroblastoma and glioblastoma tumor xenografts.[10] In this latter study, median survival, which increased from 20 (range 17–25) to 46.5 (range 29–49) days, was used as

**Correspondence to:* B. D. Ross, Department of Radiology, University of Michigan Medical School, 1150 West Medical Center Drive, MSRB III, Room 9303, Ann Arbor, MI 48109-0648, USA.
Email: bdross@umich.edu
Contract/grant sponsor: NIH/NCI; *contract grant number:* PO1CA85878; R24CA83099.
Contract/grant sponsor: NIH/NCRR; *contract grant number:* P41RR08079.

Abbreviations used: FMdC, (*E*)-2′-deoxy-2′-(fluoromethylene)cytidine; MRI, magnetic resonance imaging; ^{1}H-MRS, proton magnetic resonance spectroscopy; SRB, sulforhodamine B^{20}.

the therapeutic end-point for assessing the effect of FMdC on intracerebral human glioblastoma (D54) xenografts. FMdC has also been shown to be a strong radiosensitizing agent in culture and in animal tumor models.[11–13] The positive results of these studies have led to the initiation of phase I/II clinical trials of FMdC for solid neoplasms.[14–16]

Traditionally, promising agents like FMdC, identified through *in vitro* screening assays with brain tumor cell lines, are subsequently evaluated in rodent brain tumor models. Animal survival, colony-forming efficiency (CFE) assays of cells disaggregated from solid tumors, and measurements of excised tumor weights are then employed to quantify treatment efficacy. These methods require large groups of animals and their destructive nature precludes examination of multiple outcomes such as changes in tumor growth rate and overall survival in a single cohort. Our group has demonstrated the ability of serial MRI to quantify the cell kill elicited in individual intracerebral 9L tumors.[17–19] Our MRI-based methodology is more sensitive than traditional animal survival studies and it allows each animal to serve as its own control, thereby providing an opportunity to study inter-animal variability in treatment response. However, to date we have only applied this technique to studying responses to a single dose of a chemotherapeutic agent.

This study was designed to both examine the effectiveness of FMdC on inhibition of 9L cell proliferation *in vitro* and *in vivo*, and to study the feasibility of MRI-based measurements of cell kill elicited by daily administration of a chemotherapeutic agent. For *in vivo* studies, the effectiveness of daily i.p. administration of 15 mg/kg FMdC was evaluated. *In vivo* localized ^{1}H-MRS was also performed and revealed significant metabolic changes occurring during the treatment response. These results suggest that FMdC may be active in the treatment of malignant gliomas and demonstrates the utility of MRI-based methodology for estimating *in vivo* tumor cell kill for fractionated dosage schedules.

MATERIALS AND METHODS

In vitro evaluation of 9L cell proliferation

The antiproliferative activity of FMdC against exponentially growing 9L glioma cells in culture was studied by determining the cell growth in the presence of increasing concentrations of FMdC. Rat 9L glioma cells were grown until confluent as monolayers in modified Eagle's minimum essential medium containing 10% fetal calf serum at 37°C in a humidified atmosphere containing 95% air and 5% CO_2. Cells were harvested by trypsinization, counted, diluted in serum-free medium, plated in 96-well culture plates at a density of 1000 cells per well and allowed to grow for 24 h before treatment. Multiple concentrations of FMdC were then added to the 9L cells in culture medium for 4 days. An automated microculture assay using the protein-binding dye sulforhodamine B[20] (SRB) was utilized to quantify the toxicity of FMdC on cultured 9L cells. Under the conditions used in this study, the optical absorbance was directly proportional to the number of 9L cells. Following the 4 day exposure period, the cells were fixed, stained with SRB, and the absorbance values were obtained using a microtiter plate reader (Cayman Chemicals, Ann Arbor, MI, USA). Toxicity was assessed in terms of fractional cell survival relative to sham-treated control.

Tritiated thymidine incorporation studies

Assessment of [^{3}H]thymidine incorporation was accomplished using a modification of the Mans filter-binding method.[21] In brief, 5×10^{5} 9L cells were plated in 100 mm culture dishes. The following day, the cells were exposed to FMdC at 50 and 100 ng/ml in culture medium for a 3 day incubation period. The cells were then washed and incubated with 3 μCi/ml of [^{3}H]thymidine for 1 h at 37°C. The cells were washed again, harvested by trypsinization, and bound to filter-paper disks. Air-dried disks were washed in 5% TCA solution for 25 min, rinsed with 95% EtOH, dried for 10 min using a heat lamp and quantitated for [^{3}H]thymidine.

Induction of brain tumors

All animal experiments were approved by the University Institutional Animal Care Committee. Intracerebral brain tumors were induced in anesthetized (ketamine:xylazine 87:13 mg/kg body weight, i.p.) male Fischer 344 rats weighing between 125 and 150 g. A small skin incision over the right hemisphere was made and a high speed drill was used to create a 1 mm diameter burr hole through the skull. An inoculum of 10^{5} 9L cells in 5 μl serum-free medium was introduced into the forebrain at a depth of 3 mm through a 27 gage needle. The burr hole was then filled with bone wax to minimize the potential for extra-cerebral extension of the tumor tissue and the rats allowed to recover.

Quantitation of intracerebral tumor volumes using magnetic resonance imaging

All *in vivo* MR experiments were performed on a Varian system equipped with a 7.0 T (300 MHz proton frequency), 18.3 cm diameter horizontal bore Oxford magnet. For MRI examination, rats were anesthetized and maintained at 37°C inside the magnet using a circulating water blanket. MRI of rat brains was initiated between 8 and 10 days following 9L cell implantation and repeated every other day as described previously.[19]

In brief, the rat head was positioned inside a 4 cm diameter birdcage radiofrequency coil which was designed and constructed with ear bars to secure the position of the head during the acquisition. Multislice coronal images were acquired using a standard spin echo sequence. T_2-weighted images through the rat brain were produced using the following parameters: $TR/TE = 3500/60$ ms, FOV = 30 × 30 mm using a 128 × 128 matrix, slice thickness = 0.5 mm and slice separation = 0.8 mm. Twenty-five slices were acquired followed by acquisition of a second set of 25 slices with a slice offset of 0.4 mm, which provided a contiguous image data set of the rat brain. Tumor volumes in individual MR slices were measured and summed to yield the total tumor volume as previously described.[17]

FMdC treatment of rats with intracerebral 9L tumors

Daily treatment with FMdC was initiated after collection of three or four image data sets for each rat harboring a 9L tumor. FMdC (15 mg/kg) was dissolved in saline (0.9% NaCl) immediately prior to administration. Collection of images was continued every other day throughout the treatment period. Spectroscopy was performed 3–4 and 6–9 days after initiation of FMdC treatment in order to determine whether progressive changes in tumor metabolite levels could be correlated with retardation in tumor growth.

Cell kill calculation: fractionated dosage method

Quantitation of 9L cells killed by FMdC *in vivo* was approximated from the MRI tumor volume measurements obtained over time during the treatment protocol. Calculation of cell kill due to multiple doses was performed by an iterative fitting method using function minimization. Unlike the single dose treatment modeling method,[19] a new term which arises from the killed fraction is added at each treatment interval. For a proper approximation, the dead cell fraction at each treatment dose is determined and separated from the viable cell fraction which will undergo subsequent cell division. The post-treatment tumor volume (V_p) expressed as a function of the cell kill fraction is given by following:

$$V_p(t_i) = f_{sm}(i)V(t_1)\exp[k'(t_i - t_1)] + \Sigma V_k(i) \qquad (1)$$

where $f_{sm}(i)$ is surviving fraction of cells by the ith treatment time as expressed by $f_{sm}(i) = f_{s1} * f_{s2} * \ldots f_{s(i-1)}$, ($k' = k$) is the post treatment growth rate constant, $V(t_1)$ is tumor volume at the time of initial treatment (t_1) as described by $V(t_1) = V_0 \exp(kt_1)$, and $V_k(i)$ is the volume of tumor cells killed by the ith treatment. The last term describes the cumulative sum of dead cell volume from each treatment dose as represented in,

$$\sum_{i=1}^{n} V_k(i) = f_k(1)V(t_1) + f_k(2)V_L(2) + f_k(3)V_L(3) + \cdots + f_k(i-1)V_L(i-1) \qquad (2)$$

where $V_L(i)$ is the volume of the live cell fraction at the ith treatment time and $f_k = (1 - f_s)$. Equation (1) was used to model the effect of cell kill fractions on the tumor growth rate. Cell kill fraction, ($f_k = 1 - f_s$), by each treatment dose was determined by an iterative calculation using a MATLAB routine implemented with function minimization (FMINS).

Cell kill fraction for each treated animal was estimated by fitting post-treatment MRI volumetric data with the post-treatment growth model as estimated by eqn (1). Cell kill fraction by the treatments between MRI volume measurements (every other day) was estimated based on linearly interpolated volumes to represent daily treatment. The final cell kill estimation from each treated animal was obtained by taking an average of cell kill fraction calculated for each treatment. The treatment efficacy of FMdC was evaluated by estimating the average cell kill fraction for each daily treated animal.

Proton magnetic resonance spectroscopy

Spatially localized ^{1}H-MRS studies were obtained from untreated gliomas ($n = 4$) and FMdC treated gliomas (15 mg/kg; $n = 3$) at 6–9 days post initiation of FMdC administration. Localized *in vivo* ^{1}H spectra were acquired using a 16 mm diameter surface coil positioned above the rat head. The MRS pulse sequence restricted the ^{1}H signals to a column-shaped volume (4 × 4 or 5 × 5 mm) which was further resolved into 32 slices along the major axis of the column as previously described.[22] The non-uniformity of the surface coil transmitter B1 field was compensated by implementing adiabatic RF pulses as previously described.[22] Spectra were acquired using one-dimensional spectroscopic imaging with 32 phase encoding steps along the selected column. Shimming was accomplished on the same selected column by using a point-resolved spectroscopy (PRESS) sequence with a B_1-insensitive adiabatic pulse as a single shot method. Parameters for localized ^{1}H spectra were: $TR/TE = 2000/136$ ms, FOV = 32 mm, sweep width = 3000 Hz and spectral data points = 2K.

To differentiate lactate and lipid, spectral editing was performed on three animals as follows. Localized ^{1}H spectra were acquired from 64 mm^3 voxels using the outer volume suppression image-selected *in vivo* spectroscopy (iOVS-ISIS) method[23] in a spin-echo sequence. The 90° and 180° pulses were a solvent suppressive adiabatic pulse (SSAP) and a BIR-4 pulse, respectively. A narrowband hyperbolic secant pulse was used to invert

the lactate methine proton at 4.1 ppm in alternate excitations to allow lactate editing. Signals acquired with and without this selective 180° pulse were stored separately. Subtracting these spectra gives lactate only, whereas adding them gives normal spectra minus lactate. Spectra were acquired with the following parameters: $TR = 2300$ ms, sweep width = 3000 Hz, spectral data points = 2K, and 256 signal averages per spectrum.

All spectra were apodized with a 5 Hz line-broadening function prior to Fourier transformation. Resonance areas were quantified with a spectral deconvolution routine.

RESULTS

In vitro studies

Survival studies of 9L cells following a 4 day exposure to increasing concentrations of FMdC revealed dose-dependent toxicity with an EC_{50} of 40 ng/ml (155 nM) [$n = 8$, Fig. 1(A)]. To further examine FMdC-inhibition of 9L cell proliferation and DNA synthesis, [^{3}H]thymidine incorporation was measured in cells exposed to FMdC at 50 and 100 ng/ml for 3 days. Figure 1(B) demonstrates an FMdC dose-dependent decrease in [^{3}H]thymidine incorporation relative to untreated control cells.

MRI of untreated and FMdC treated 9L tumors

A series of coronal T_2-weighted MR images of intracranial 9L tumors is shown in Fig. 2. Figure 2(A–E) shows images of a rat brain harboring an untreated 9L tumor at 13, 15, 17, 19 and 21 days post-implantation, respectively. The expanding tumor mass is distinctively evident as a well-demarcated hyperintense region allowing for accurate quantitation of tumor volumes over time. Images of a representative tumor treated with FMdC (15 mg/kg, daily i.p.) are shown in the images in Fig. 2(F–J), which were acquired on days 19, 21, 23, 25 and 28 days post-cell implantation, respectively. Following initiation of daily doses of FMdC on day 21 [Fig. 2(G)], there is a notable increase in the heterogeneity of the tumor MR signal manifested as regions of low-signal necrosis centrally and more peripheral increases in intensity probably representing treatment-induced intratumoral edema. Note that there is a persistent and progressive increase in the cross-sectional area of the tumor while it is undergoing treatment, although the tumor is slowing in growth rate.

As we previously reported, the 9L tumor grows exponentially throughout the entire lifespan of the rat.[17] This observation is important because it allows intracranial tumor doubling times to be determined prior to treatment in individual animals. This feature allows each rat to serve as its own control; the effect of treatment can be quantified as the degree of deviation from exponential growth using an appropriate mathematical model. Figure 3 reveals the growth of a representative intracranial 9L tumor treated with daily FMdC at 15 mg/kg. The pre-treatment tumor doubling time was calculated to be 54 h for the tumor shown in Fig. 3 (solid squares and hashed line). Following treatment initiation, a slowing of tumor growth rate was observed and is reflected in the deviation of the growth curve (open squares) from the pre-treatment exponential growth rate. The treated tumor shown in Fig. 3 had a 91% decrease in growth rate as calculated using the last three volumetric time points (open squares). A summary of pre-treatment tumor doubling time and percent growth inhibition after treatment of rats with 15 mg/kg FMdC is given in Table

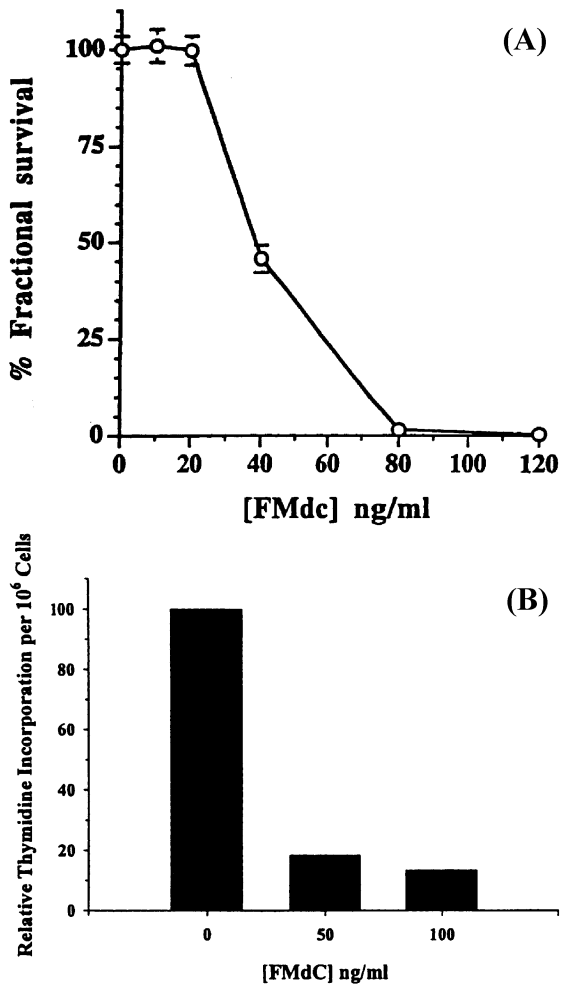

Figure 1. (A) Effect of FMdC on 9L cell growth *in vitro*. Cells were incubated for 4 days in the presence of increasing concentrations of FMdC. Cytotoxicity was measured using the SRB assay and data expressed as percent survival relative to control cells ($n = 8 \pm$ SE). (B) Effects of 9L cell exposure to FMdC (50 and 100 ng/ml) for 3 days on [^{3}H]thymidine incorporation relative to control

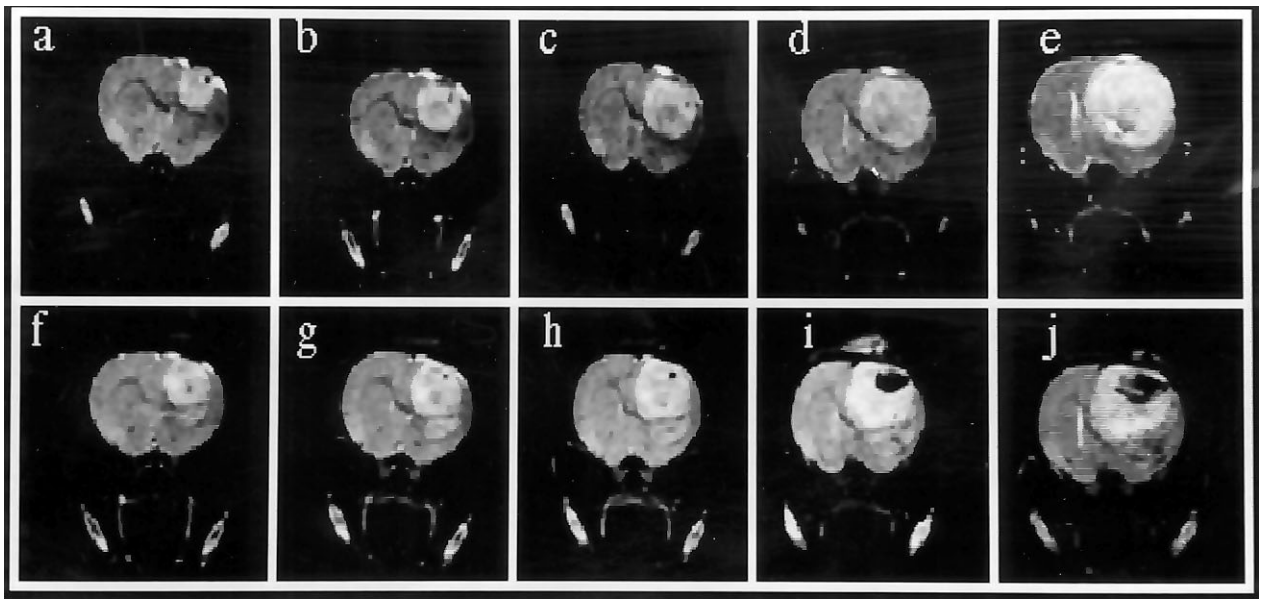

Figure 2. Coronal T_2-weighted MR images of rat brains with intracranial 9L tumors. Images in top row (A–E) were obtained from an untreated rat on days, 13, 15, 17, 19 and 21 days post-cell implantation. Bottom images (F–J) were obtained from an FMdC-treated rat (daily FMdC treatments were initiated on day 21) on days 19, 21, 23, 25 and 27 post cell implantation. Images from treated 9L tumors revealed increasing inhomogeneity of the signal intensity within the tumor mass as the treatments continued as compared to the tumor images of the untreated rat

1. Four out of seven rats treated with 15 mg/kg FMdC showed a significant change in tumor growth rate as calculated from the MR images, with a mean growth inhibition for the responsive group of 91%.

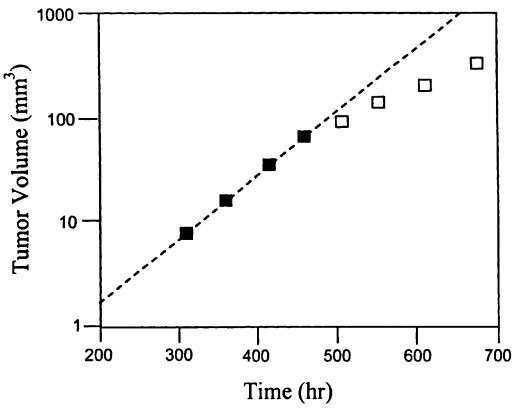

Figure 3. Plot of MRI-determined intracerebral 9L tumor volumes for pre-treatment (solid squares) and post-initiation of daily FMdC treatments (open squares) vs hours post implantation of 9L cells. Rats received 15 mg/kg FMdC i.p. once daily which began following the determination of the last pre-treatment volume measurement (solid square). The volume data obtained were from the images of the rat shown in Fig. 2(F–J). The post-treatment data (open squares) exhibit a progressive decrease in tumor growth rate as administration of FMdC continues

Calculation of *in vivo* tumor cell kill

Quantification of tumor cell kill using the MRI volumetric data was accomplished using the expression given by eqn (1). In order to demonstrate the effects of multiple treatments over a range of cell kills (0.1–2.0 log kill/dose), theoretical tumor growth curves were modeled using eqn (1) and plotted in Fig. 4. Assumptions in this model included a pre-treatment doubling time of 50 h, a constant cell kill fraction (f_k) induced by each daily dose of FMdC, and no reduction in tumor volumes following cell kill attributable to shrinkage or removal of cellular debris. Unlike the single dose method,[17] these curves exhibit the cumulative effect of a multi-dose-treatment regimen, which contributes to a continual slowing of tumor growth throughout the duration of treatment. By fitting the experimental post-treatment tumor volume data obtained from MRI measurements to the above model, estimation of daily cell kill values due to FMdC was accomplished. As summarized in Table 1, tumors which responded to daily FMdC treatments of 15 mg/kg incurred a cell kill of 0.1–0.2 log (20%) at each dose. At this dosage schedule the treatment was well tolerated by the rats and there were no observable side effects.

Effects of FMdC treatment on the ^{1}H MR spectra of intracerebral 9L tumors

A series of spatially localized *in vivo* ^{1}H spectra acquired along a column positioned through the center of the

Table 1. Summary of the effects of FMdC on intracerebral 9L tumors

Rat no.	FMdC dose (mg/kg)[a]	Pre-treatment tumor T_d[b]	Percentage growth inhibition[c]	Average daily log kill[d]
1	15	54	91	0.1
2	15	63	73	0.1
3	15	70	0	0
4	15	59	0	0
5	15	63	0	0
6	15	56	80	0.1
7	15	40	120	0.2

[a] Administered i.p. once daily to rats.
[b] Determined from the growth of intracerebral 9L tumors as assessed by MRI.
[c] Tumor growth inhibition was estimated from the pre- and post-treatment tumor T_d. Post-treatment tumor T_d values were determined by fitting the post-treatment volumetric data.
[d] Determined using eqn (1) to fit post-treatment volumetric data.

tumor mass along the two hemispheres are displayed in Fig. 5. The first series of spectra were acquired from a rat brain with an untreated 9L tumor [Fig. 5(A)]. The contralateral side is characterized by resonances from *N*-acetyl aspartate (NAA), creatine (Cr) and choline-containing compounds (Ch) at 2.0, 3.0 and 3.2 ppm, respectively. This representative example of ^{1}H spectra from an untreated 9L tumor reveals an absence of NAA, a decrease in the level of creatine, and an increase in the choline resonance in the tumor. No apparent changes in tumor metabolite levels were evident during normal growth of untreated intracerebral 9L tumors ($n = 4$, data not shown). Shown in Fig. 5(B) and (C) are spectra acquired from a rat treated with FMdC (15 mg/kg, i.p.) at 6 and 9 days, respectively. The spectra displayed in Fig. 5(B) and (C) are from the same representative treated rat

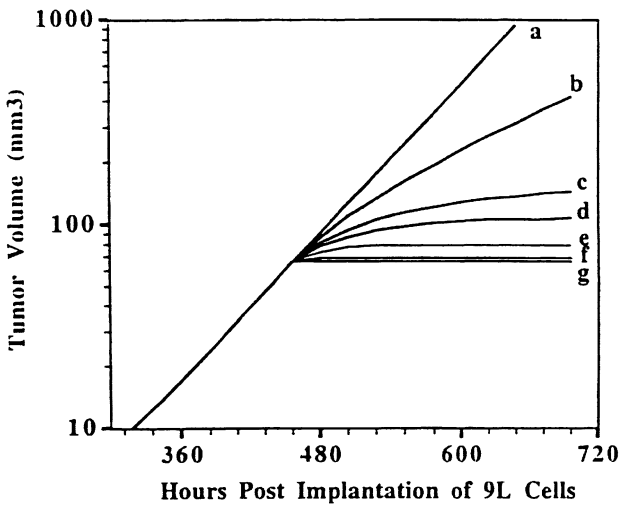

Figure 4. Theoretical plot of tumor growth curves and the effects of daily treatments generated using eqn (1). Curve a represents untreated tumor growth and curves b, c, d, e, f and g were modeled using a constant log cell kill of 0.1, 0.2, 0.3, 0.5, 1 and 2, respectively. The tumor volumes were calculated assuming a pre-treatment T_d of 50 h and the volume of the intracranial tumor is not reduced following cell kill due to resorption of cellular debris

shown in Figs 2(F–J) and 3. Note the relative increase in the lipid–lactate resonance in the treated tumor and the reduction in the tumor choline resonance.

Resonance signals from NAA, creatine, choline as well as the lipid + lactate peak at 1.3 ppm were integrated to quantify the relative metabolite levels. The relative signal intensities of each metabolite were normalized to NAA in the contralateral hemisphere, averaged and summarized in Table 2. The untreated 9L tumor exhibited an increase in choline and a marked drop in creatine levels as compared to the contralateral hemisphere. At 6–9 days post initiation of daily FMdC treatments, an increase in the lipid + lactate peak (1.3 ppm) from 0.22 ± 0.10 ($n = 3, \pm$ SE) to 0.86 ± 0.31 was observed in the 9L tumor spectra. Furthermore, changes were observed at 6–9 days post treatment initiation in the choline resonance area which decreased from the untreated value of 0.31 ± 0.03 to 0.16 ± 0.05. Also note that FMdC treatment lowered the elevated Cho/Cr ratio of the 9L glioma.

Homonuclear spectral editing experiments were carried out to separate the lipid and lactate in the peak at 1.3 ppm. The lactate-edited spectrum shown in Fig. 6 was acquired from a representative intracerebral 9L tumor ($n = 3$) after 2 weeks of FMdC treatment. The lower panel is the summation spectrum with the lactate signal suppressed by a selective 180° inversion pulse. The upper panel is the complementary processed difference spectrum which shows the lactate resonance. These spectra show that lactate was the predominant contributor to the 1.3 ppm signal.

DISCUSSION

The results of this study provide further evidence that FMdC may be an active agent against high-grade gliomas and demonstrates the sensitivity of serial MRI measurements of tumor cell kill for quantitating fractionated dosage schedules. *In vitro* studies demonstrated that cultured 9L tumor cells were sensitive to FMdC with an

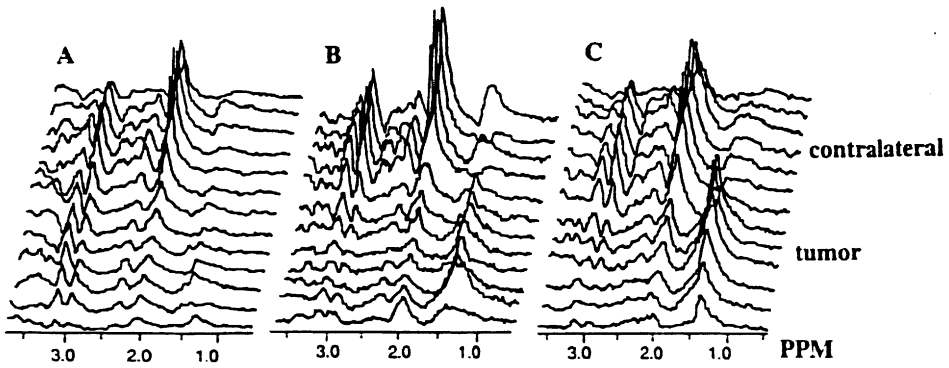

Figure 5. Spatially localized ^{1}H magnetic resonance spectra obtained from a rat brain harboring an (A) untreated intracranial 9L tumor and a treated glioma on the (B) sixth and (C) ninth day following initiation of daily treatments with FMdC (15 mg/kg, i.p.). Each series of spectra were obtained from 25 μl voxels along a column through the rat brain. In the contralateral side, resonances were observed corresponding to NAA, creatine and choline at 2.0, 3.0 and 3.2 ppm, respectively. Untreated 9L tumors showed absence of NAA, increased choline and decreased creatine as compared with the contralateral brain spectra. FMdC treated tumors showed a progressive increase in the lipid + lactate resonance intensity (1.3 ppm) and decreased choline intensity on days 6 and 9 of treatment

EC_{50} of 155 nM. These results are similar to previously published *in vitro* studies of other brain tumor cell lines which exhibited EC_{50}s between 30 and 90 nM.[10] The [^{3}H]thymidine incorporation studies demonstrate potent inhibition of DNA synthesis in cultures exposed to FMdC for 3 days. The EC_{50} was not calculated in these experiments, but we observed an approximate 80% inhibition of DNA synthesis by 50 ng/ml (194 nM) of FMdC. The discrepancy between the [^{3}H]thymidine incorporation and SRB cell survival assays may be attributable to repair of sub-lethal damage induced by FMdC. Further investigation is required to address this observation.

The potential for clinical efficacy of FMdC against human gliomas is further supported by our *in vivo* data which demonstrate inhibition of intracerebral 9L tumor growth. This effect ranged from a 74–120% inhibition in growth rate in responders to the 15 mg/kg dose schedule. Piepmeier has previously reported enhanced survival in nude mice harboring intracerebral D54 human glioma xenografts treated bi-weekly with 100 mg/kg FMdC i.p.[10] Taken together, the results of these studies suggest that FMdC is able to penetrate intracerebral tumors at cytotoxic concentrations. Our current study using MRI also reveals the importance of knowing the size (volume) of the tumor at the time of treatment initiation, especially for the case of fractionated dosage schedules. Tumors in the rat cranial cavity are typically in the range of 200–300mm^{3} when the animal becomes moribund. Since fractionated doses of FMdC only produced small daily cell kill values, initiation of treatment at smaller tumor volumes would provide for more time for the additive therapeutic doses to translate into improved survival. Optimization of therapeutic efficacy can be achieved by using noninvasive MRI to evaluate the timing of treatment initiation along with the effects of dose escalation and frequency.

This study further demonstrates the sensitivity of MRI-based measurement of *in vivo* tumor cell kill. We have previously shown that MRI provides an accurate means of quantifying tumor volume, growth rates and changes in tumor volume growth following treatment with a single dose of a chemotherapeutic agent.[19] Owing to the complexity of cell growth kinetics, an accurate modeling and calculation of cell kill fraction by each treatment dose for a given multi-treatment protocol is a far more challenging task. We simplified our mathematical model by assuming no tumor volume reduction due to removal of dead cell debris and were thereby able to

Table 2. Average normalized *in vivo* metabolite levels obtained using ^{1}H-MRS

	Choline[a]	Creatine[a]	Choline/creatine	1.3 ppm resonance[a]
Contralateral brain ($n = 4$)	0.23 ± .02	0.42 ± .03	0.55	0.08 ± .04
Untreated 9L tumor ($n = 4$)	0.31 ± .03	0.13 ± .02	2.38	0.22 ± .10
Treated 9L tumor[b] ($n = 3$)	0.16 ± .05	0.11 ± .03	1.45	0.86 ± .31

[a] Values are normalized relative to the intensity of the normal brain NAA peak.
[b] Spectra were acquired from between 6 and 9 days following initiation of daily administration of FMdC (15 mg/kg, i.p.).

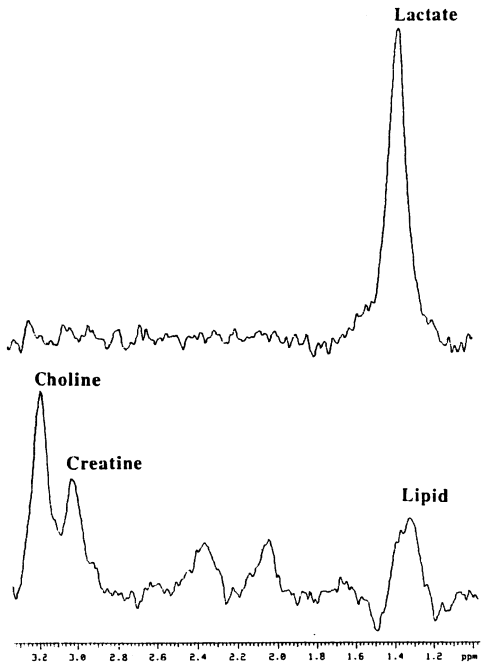

Figure 6. Localized, homonuclear editing of lactate in ^{1}H magnetic resonance spectra of a 9L rat brain tumor after 2 weeks of treatment with FMdC. The lactate signal is removed from the lower spectrum by summation of spectra acquired with and without the selective lactate pulse. The lactate signal is isolated in the upper spectrum by subtracting spectra with and without the selective lactate pulse

provide quantitative estimates of the small cell kills elicited by each dose of a fractionated therapy. Daily doses of FMdC administered in this study induced log cell kills on the order of 0.1 for responders. Given the lack of a statistically significant prolongation of animal survival (data not shown), it is impressive to note the MRI methodology documented therapeutic effects that would have otherwise been overlooked. This methodology has the potential to be of great value in evaluating novel interventions in which multiple factors must be optimized in order to achieve a significant therapeutic benefit. Animal model studies of such treatment modalities, like suicide gene therapy, which requires optimization of gene and prodrug delivery, could be greatly facilitated by sensitive MRI-based assays of therapeutic effects.

Localized ^{1}H-MRS is clearly emerging as a valuable tool in the evaluation of efficacy of treatments for primary brain tumors. Biochemical changes in gliomas associated with treatment response have recently been identified in ^{1}H-MRS studies of animal models,[24,25] and in glioma patients treated with tamoxifen[26] or radiation therapy.[27] In this study we observed a pattern of changes in metabolite levels in FMdC-treated 9L gliomas, characterized by progressive decreases in choline/creatine ratio and increases in the 1.3 ppm lipid/lactate resonance peak intensity compared with untreated tumor spectra. The results of the spectral editing experiment suggest that an increase in tumor lactate is the predominant contributor to the increased signal at 1.3 ppm. These changes correlated with growth retardation detected by MRI volume studies and with progressive increases in the heterogeneity of tumor contrast as shown in Fig. 3(F–J). Our results are consistent with those of others showing decreased choline in areas of human gliomas responding to radiation therapy.[28] The observed increases in tumor lactate may be due to increased glycolytic activity or decreased lactate removal in the face of treatment-induced changes in tumor neovasculature. Further study will be required to understand the mechanistic basis for the observed changes in tumor ^{1}H-MRS signals elicited by FMdC.

In conclusion, these results provide good evidence for continuing the evaluation of FMdC as a chemotherapeutic agent for high-grade glioma. FMdC's previously documented potency as a radiation sensitizer[11–13] also deserves further evaluation in brain tumor models since improved local control of these tumors with more effective radiotherapy may improve patient outcome. Moreover, this study adds to the growing body of work demonstrating the sensitivity of serial MRI and MRS measurements for studying tumor responses to therapy. Moreover, molecular imaging[29] is emerging from molecular biology and imaging sciences as an important new avenue for drug development in pre-clinical animal model studies. This field employs a variety of imaging modalities including magnetic resonance imaging (MRI),[24,25,30–42] positron emission tomography (PET) and single photon emission tomography (SPECT),[42–51] X-ray computed tomography (CT)[52,53] and optical methods.[30,33,54–66] These capabilities, along with the rapid growth of new imaging reporters for the detection of molecular events should dramatically change the approaches used to evaluate new therapeutic strategies. For example, in this current study, the effects of FMdC on glucose metabolism could also be evaluated by ^{18}F-fluorodeoxyglucose PET studies. This would provide further opportunity to investigate the mechanism of the observed increased lactate concentrations within the 9L brain tumor during treatment. Overall, integration of imaging and spectroscopic studies into the drug development process will yield invaluable insights into the mechanism of action and/or the therapeutic effectiveness of agents under study.

Acknowledgements

The authors would like to thank Hoechst Marion Roussel Research Institute, Hoechst Marion Roussel, Inc. for supplying the FMdC used in these experiments. This work was supported by research grants from the NIH/NCI: PO1CA85878 and R24CA83099.

REFERENCES

1. Shapiro WR, Shapiro JR, Walker RW. Central nervous system. In Clinical Oncology, Abeloff MD, Armitage JO, Lichter AS, Niederhuber JE (eds). Churchill Livingstone: New York, 2000; 1103–1192.
2. Stewart LA. Chemotherapy in adult high-grade glioma: a systematic review and meta-analysis of individual patient data from 12 randomised trials. *Lancet* 2002; **359**: 1011–1018.
3. Giese A, Westphal M. Treatment of malignant glioma: a problem beyond the margins of resection. *J. Cancer Res. Clin. Oncol.* 2001; **127**: 217–225.
4. McCarthy JR, Matthews DP, Stemerick DM, Huber EW, Bey P, Lippert BJ, Snyder RD, Sunkara PS. Stereospecific method to *E* and *Z* terminal fluoro olefins and its application to the synthesis of 2′-deoxy-2′-fluoromethylene nucleosides as potential inhibitors of ribonucleotide diphosphate reductase. *J. Am. Chem. Soc.* 1991; **113**: 7439–7440.
5. Kanazawa J, Takahashi T, Akinaga S, Tamaoki T, Okabe M. The relationship between the antitumor activity and the ribonucleotide reductase inhibitory activity of (*E*)-2′-deoxy-2′-(fluoromethylene) cytidine, MDL 101,731. *Anticancer Drugs* 1998; **9**: 653–657.
6. Zhou Y, Achanta G, Pelicano H, Gandhi V, Plunkett W, Huang P. Action of (*E*)-2′-deoxy-2′-(fluoromethylene)cytidine on DNA metabolism: incorporation, excision, and cellular response. *Mol. Pharmac.* 2002; **61**: 222–229.
7. Bitonti AJ, Dumont JA, Bush TL, Cashman EA, Cross-Doersen DE, Wright PS, Matthews DP, McCarthy JR, Kaplan DA. Regression of human breast tumor xenografts in response to (*E*)-2′-deoxy-2′-(fluoromethylene)cytidine, an inhibitor of ribonucleoside diphosphate reductase. *Cancer Res.* 1994; **54**: 1485–1490.
8. Wright PS, Cross-Doersen D, Th'ng JP, Guo XW, Crissman HA, Bradbury EM, Montgomery LR, Thompson FY, Loudy DE, Johnston JO, Bitonti AJ. A ribonucleotide reductase inhibitor, MDL 101,731, induces apoptosis and elevates TRPM-2 mRNA levels in human prostate tumor xenografts. *Exp. Cell Res.* 1996; **222**: 54–60.
9. Bitonti AJ, Bush TL, Lewis MT, Sunkara PS. Response of human colon and prostate tumor xenografts to (*E*)-2′-deoxy-2′-(fluoromethylene) cytidine, an inhibitor of ribonucleotide reductase. *Anticancer Res.* 1995; **15**: 1179–1182.
10. Piepmeier JM, Rabidou N, Schold SC Jr, Bitonti AJ, Prakash NJ, Bush TL. *In vitro* and *in vivo* inhibition of glioblastoma and neuroblastoma with MDL101731, a novel ribonucleoside diphosphate reductase inhibitor. *Cancer Res.* 1996; **56**: 359–361.
11. Snyder RD. Effect of 2′-deoxy-2′-(fluoromethylene) cytidine on the ultraviolet and X-ray sensitivity of HeLa cells. *Oncol. Res.* 1994; **6**: 177–182.
12. Sun LQ, Li YX, Guillou L, Mirimanoff RO, Coucke PA. Antitumor and radiosensitizing effects of (*E*)-2′-deoxy-2′-(fluoromethylene) cytidine, a novel inhibitor of ribonucleoside diphosphate reductase, on human colon carcinoma xenografts in nude mice. *Cancer Res.* 1997; **57**: 4023–4028.
13. Sun LQ, Li YX, Guillou L, Coucke PA. (*E*)-2′-deoxy-2′-(fluoromethylene) cytidine potentiates radioresponse of two human solid tumor xenografts. *Cancer Res.* 1998; **58**: 5411–5417.
14. Seley KL. Tezacitabine Hoechst Marion Roussel. *Curr. Opin. Invest. Drugs* 2000; **1**: 135–140.
15. Noriyuki M, Shunichi N, Kouji T, Nobuhide T, Tomonori H, Takashi Y, Norialki K, Takashi K, Satoshi K, Shinzoh K. Phase I and pharmacologic study of oral (*E*-2′-deoxy-2′ (fluoromethylene) cytidine on a daily ×5-day schedule. *Invest. New Drugs* 1999; **16**: 245–254.
16. Rodriguez GL, Brooks DJ, Burtness BA. Phase I clinical trials of intravenous 2′-deoxy-2′-(fluoromethylene) cytidine (FMdC) in patients with advanced solid tumors. *Proc. Am. Soc. Clin. Oncol.* 1999; **18**: 15–18.
17. Kim B, Chenevert TL, Ross BD. Growth kinetics and treatment response of the intracerebral rat 9L brain tumor model: a quantitative *in vivo* study using magnetic resonance imaging. *Clin. Cancer Res.* 1995; **1**: 643–650.
18. Ross BD, Kim B, Davidson BL. Assessment of ganciclovir toxicity to experimental intracranial gliomas following recombinant adenoviral-mediated transfer of the herpes simplex virus thymidine kinase gene by magnetic resonance imaging and proton magnetic resonance spectroscopy. *Clin. Cancer Res.* 1995; **1**: 651–657.
19. Ross BD, Zhao YJ, Neal ER, Stegman LD, Ercolani M, Ben-Yoseph O, Chenevert TL. Contributions of cell kill and posttreatment tumor growth rates to the repopulation of intracerebral 9L tumors after chemotherapy: an MRI study. *Proc. Natl Acad. Sci. USA* 1998; **95**: 7012–7017.
20. Rubinstein LV, Shoemaker RH, Paull KD, Simon RM, Tosini S, Skehan P, Scudiero DA, Monks A, Boyd MR. Comparison of in vitro anticancer-drug-screening data generated with a tetrazolium assay versus a protein assay against a diverse panel of human tumor cell lines. *J. Natl Cancer Inst.* 1990; **82**: 1113–1118.
21. Mans RJ, Novelli GD. Measurement of the incorporation of radioactive amino acids into protein by a filter-paper disk method. *Arch. Biochem. Biophys.* 1961; **94**: 48–53.
22. Ross BD, Merkle H, Hendrich K, Staewen RS, Garwood M. Spatially localized *in vivo* ^{1}H magnetic resonance spectroscopy of an intracerebral rat glioma. *Magn. Reson. Med.* 1992; **23**: 96–108.
23. de Graaf RA, Luo Y, Terpstra M, Garwood M. Spectral editing with adiabatic pulses. *J. Magn. Reson. B* 1995; **109**: 184–193.
24. Evelhoch JL, Gillies RJ, Karczmar GS, Koutcher JA, Maxwell RJ, Nalcioglu O, Raghunand N, Ronen SM, Ross BD, Swartz HM. Applications of magnetic resonance in model systems: cancer therapeutics. *Neoplasia* 2000; **2**: 152–165.
25. Gillies RJ, Bhujwalla ZM, Evelhoch J, Garwood M, Neeman M, Robinson SP, Sotak CH, Van Der Sanden B. Applications of magnetic resonance in model systems: tumor biology and physiology. *Neoplasia* 2000; **2**: 139–151.
26. Preul MC, Caramanos Z, Villemure JG, Shenouda G, LeBlanc R, Langleben A, Arnold DL. Using proton magnetic resonance spectroscopic imaging to predict in vivo the response of recurrent malignant gliomas to tamoxifen chemotherapy. *Neurosurgery* 2000; **46**: 306–318.
27. Ng SH, Ko SF, Chen WC, Tang LM, Chang CN, Wai YY, Wan YL. Proton magnetic resonance spectroscopy of cerebral glioma after irradiation. *Chang Gung Med. J.* 2001; **24**: 708–716.
28. Nelson SJ, Vigneron DB, Dillon WP. Serial evaluation of patients with brain tumors using volume MRI and 3D 1H MRSI. *NMR Biomed.* 1999; **12**: 123–138.
29. Hoffman JM. Imaging in cancer: a National Cancer Institute "extraordinary opportunity". *Neoplasia* 2000; **2**: 5–8.
30. Rehemtulla A, Hall DE, Stegman LD, Chen G, Bhojani MS, Chenevert TL, Ross BD. Molecular imaging of gene expression and efficacy following adenoviral-mediated brain tumor gene therapy. *Mol. Imag.* 2002; **1**: 43–55.
31. Bremer C, Tung CH, Weissleder R. *In vivo* molecular target assessment of matrix metalloproteinase inhibition. *Nat. Med.* 2001; **7**: 743–748.
32. Chinnaiyan AM, Prasad U, Shankar S, Hamstra DA, Shanaiah M, Chenevert TL, Ross BD, Rehemtulla A. Combined effect of tumor necrosis factor-related apoptosis-inducing ligand and ionizing radiation in breast cancer therapy. *Proc. Natl Acad. Sci. USA* 2000; **97**: 1754–1759.
33. Rehemtulla A, Stegman LD, Cardozo SJ, Gupta S, Hall DE, Contag CH, Ross BD. Rapid and quantitative assessment of cancer treatment response using in vivo bioluminescence imaging. *Neoplasia* 2000; **2**: 491–495.
34. Kurhanewicz J, Vigneron DB, Nelson SJ. Three-dimensional magnetic resonance spectroscopic imaging of brain and prostate cancer. *Neoplasia* 2000; **2**: 166–189.
35. Kaplan O, Firon M, Vivi A, Navon G, Tsarfaty I. HGF/SF activates glycolysis and oxidative phosphorylation in DA3 murine mammary cancer cells. *Neoplasia* 2000; **2**: 365–377.
36. Fleige G, Nolte C, Synowitz M, Seeberger F, Kettenmann H, Zimmer C. Magnetic labeling of activated microglia in experimental gliomas. *Neoplasia* 2001; **3**: 489–499.
37. Bogdanov A, Matuszewski L, Bremer C, Petrovsky A, Weissleder R. Oligomerization of paramagnetic substrates result in signal amplification and can be used for MR imaging of molecular targets. *Mol. Imag.* 2002; **1**: 16–23.
38. Hogemann D, Josephson L, Weissleder R, Basilion JP. Improvement of MRI probes to allow efficient detection of gene expression. *Bioconjug. Chem.* 2000; **11**: 941–946.
39. Bhujwalla ZM, Artemov D, Natarajan K, Ackerstaff E, Solaiyappan M. Vascular differences detected by MRI for metastatic versus

nonmetastatic breast and prostate cancer xenografts. *Neoplasia* 2001; **3**: 143–153.
40. Pilatus U, Ackerstaff E, Artemov D, Mori N, Gillies RJ, Bhujwalla ZM. Imaging prostate cancer invasion with multi-nuclear magnetic resonance methods: the Metabolic Boyden Chamber. *Neoplasia* 2000; **2**: 273–279.
41. Chenevert TL, Stegman LD, Taylor JM, Robertson PL, Greenberg HS, Rehemtulla A, Ross BD. Diffusion magnetic resonance imaging: an early surrogate marker of therapeutic efficacy in brain tumors. *J. Natl Cancer Inst.* 2000; **92**: 2029–2036.
42. Stegman LD, Rehemtulla A, Beattie B, Kievit E, Lawrence TS, Blasberg RG, Tjuvajev JG, Ross BD. Noninvasive quantitation of cytosine deaminase transgene expression in human tumor xenografts with *in vivo* magnetic resonance spectroscopy. *Proc. Natl Acad. Sci. USA* 1999; **96**: 9821–9826.
43. Ponomarev V, Doubrovin M, Lyddane C, Beresten T, Balatoni J, Bornman W, Finn R, Akhurst T, Larson S, Blasberg R, Sadelain M, Tjuvajev JG. Imaging TCR-dependent NFAT-mediated T-cell activation with positron emission tomography *in vivo*. *Neoplasia* 2001; **3**: 480–488.
44. Gambhir SS, Herschman HR, Cherry SR, Barrio JR, Satyamurthy N, Toyokuni T, Phelps ME, Larson SM, Balatoni J, Finn R, Sadelain M, Tjuvajev J, Blasberg R. Imaging transgene expression with radionuclide imaging technologies. *Neoplasia* 2000; **2**: 118–138.
45. Tjuvajev JG, Joshi A, Callegari J, Lindsley L, Joshi R, Balatoni J, Finn R, Larson SM, Sadelain M, Blasberg RG. A general approach to the non-invasive imaging of transgenes using cis-linked herpes simplex virus thymidine kinase. *Neoplasia* 1999; **1**: 315–320.
46. Gambhir SS, Barrio JR, Phelps ME, Iyer M, Namavari M, Satyamurthy N, Wu L, Green LA, Bauer E, MacLaren DC, Nguyen K, Berk AJ, Cherry SR, Herschman HR. Imaging adenoviral-directed reporter gene expression in living animals with positron emission tomography. *Proc. Natl Acad. Sci. USA* 1999; **96**: 2333–2338.
47. Mankoff DA, Dehdashti F, Shields AF. Characterizing tumors using metabolic imaging: PET imaging of cellular proliferation and steroid receptors. *Neoplasia* 2000; **2**: 71–88.
48. Dyszlewski M, Blake HM, Dahlheimer JL, Pica CM, Piwnica-Worms D. Characterization of a novel 99mTc-carbonyl complex as a functional probe of MDR1 P-glycoprotein transport activity. *Mol. Imag.* 2002; **1**: 24–36.
49. Hackman T, Doubrovin M, Balatoni J, Beresten T, Ponomarev V, Beattie B, Finn R, Bornmann W, Blasberg R, Tjuvajev JGG. Imaging expression of cytosine deaminase—herpes virus thymidine kinase fusion gene (CD/TK) expression with [124I]FIAU and PET. *Mol. Imag.* 2002; **1**: 36–42.
50. Hay RV, Cao B, Skinner RS, Wang L-M, Su Y, Resau JH, Woude GFV, Gross MD. Radioimmunoscintigraphy of tumors autocrine for human met and hepatocyte growth factor/scatter factor. *Mol. Imag.* 2002; **1**: 56–62.
51. Burt BM, Humm JL, Kooby DA, Squire OD, Mastorides S, Larson SM, Fong Y. Using positron emission tomography with [(18)F]FDG to predict tumor behavior in experimental colorectal cancer. *Neoplasia* 2001; **3**: 189–195.
52. Kristensen CA, Hamberg LM, Hunter GJ, Roberge S, Kierstead D, Wolf GL, Jain RK. Changes in vascularization of human breast cancer xenografts responding to antiestrogen therapy. *Neoplasia* 1999; **1**: 518–525.
53. Paulus MJ, Gleason SS, Kennel SJ, Hunsicker PR, Johnson DK. High resolution X-ray computed tomography: an emerging tool for small animal cancer research. *Neoplasia* 2000; **2**: 62–70.
54. Sameni M, Moin K, Sloane BF. Imaging proteolysis by living human breast cancer cells. *Neoplasia* 2000; **2**: 496–504.
55. Jacobs A, Breakefield XO, Fraefel C. HSV-1-based vectors for gene therapy of neurological diseases and brain tumors: part I. HSV-1 structure, replication and pathogenesis. *Neoplasia* 1999; **1**: 387–401.
56. Fujimoto JG, Pitris C, Boppart SA, Brezinski ME. Optical coherence tomography: an emerging technology for biomedical imaging and optical biopsy. *Neoplasia* 2000; **2**: 9–25.
57. Tromberg BJ, Shah N, Lanning R, Cerussi A, Espinoza J, Pham T, Svaasand L, Butler J. Non-invasive in vivo characterization of breast tumors using photon migration spectroscopy. *Neoplasia* 2000; **2**: 26–40.
58. Vajkoczy P, Ullrich A, Menger MD. Intravital fluorescence videomicroscopy to study tumor angiogenesis and microcirculation. *Neoplasia* 2000; **2**: 53–61.
59. Ramanujam N. Fluorescence spectroscopy of neoplastic and non-neoplastic tissues. *Neoplasia* 2000; **2**: 89–117.
60. Pedersen MW, Holm S, Lund EL, Hojgaard L, Kristjansen PE. Coregulation of glucose uptake and vascular endothelial growth factor (VEGF) in two small-cell lung cancer (SCLC) sublines *in vivo* and *in vitro*. *Neoplasia* 2001; **3**: 80–87.
61. Kragh M, Quistorff B, Lund EL, Kristjansen PE. Quantitative estimates of vascularity in solid tumors by non-invasive near-infrared spectroscopy. *Neoplasia* 2001; **3**: 324–330.
62. Vordermark D, Shibata T, Martin Brown J. Green fluorescent protein is a suitable reporter of tumor hypoxia despite an oxygen requirement for chromophore formation. *Neoplasia* 2001; **3**: 527–534.
63. Edinger M, Sweeney TJ, Tucker AA, Olomu AB, Negrin RS, Contag CH. Noninvasive assessment of tumor cell proliferation in animal models. *Neoplasia* 1999; **1**: 303–310.
64. Contag CH, Jenkins D, Contag PR, Negrin RS. Use of reporter genes for optical measurements of neoplastic disease *in vivo*. *Neoplasia* 2000; **2**: 41–52.
65. Padera TP, Stoll BR, So PTC, Jain RK. Conventional and high-speed intravital multiphoton laser scanning microscopy of microvasculature, lymphatics, and leukocyte-endothelial interactions. *Mol. Imag.* 2002; **1**: 9–15.
66. Hawrysz DJ, Sevick-Muraca EM. Developments toward diagnostic breast cancer imaging using near-infrared optical measurements and fluorescent contrast agents. *Neoplasia* 2000; **2**: 388–417.

